Temperature Distribution in Non-Zero Circulation Swirling Jet in Crossflow

Weerin Wangjiraniran and Asi Bunyajitradulya
Fluid Mechanics Research Laboratory, Department of Mechanical Engineering
Faculty of Engineering, Chulalongkorn University
Bangkok 10330, Thailand
Tel. 02-218-6645; Fax. 02-252-2889
Email: basi@chula.ac.th
URL: http://www.eng.chula.ac.th/~fmeabj

Abstract

Non-zero circulation swirling jet in crossflow is studied. Heated swirling jet generated from a rotating pipe is used and the temperature distribution in the near field downstream of the jet is surveyed. The experiment is conducted at a fixed effective jet-to-crossflow momentum ratio of 4.1 and swirl ratio ranged from 0 (no swirl) to 0.82. The results indicate that, within the present range of parameters, swirl has little influence on the global parameters, namely, the maximum centerplane-temperature trajectory and decay, in comparison to the effect of the effective jet-to-crossflow momentum ratio. On the other hand, detailed measurements of temperature distribution in the crossplane reveal the pronounced effect of swirl on the jet structure. Specifically, swirl causes asymmetry in the jet structure and in the temperature distribution within the jet, creating a region of high temperature and temperature gradient on the *suction* side and a corresponding region of low temperature and temperature gradient on the *pressure* side. This is attributed to the development, and the contrasting effect of swirl velocity on the development, of a skew mixing layer on each lateral edge of the jet. The degree of asymmetry is observed to increase with swirl. Nonetheless, it is also observed that, albeit the effect of swirl on the asymmetry of temperature distribution within the jet, the low temperature envelop of the jet is relatively symmetric. In this regard, this, together with the fact that the global parameters are little influenced by swirl, suggests to the distinctive roles and effects of the effective jet-to-crossflow momentum ratio and of swirl.

1. Introduction

A jet in a crossflow is a flow of many technological applications. It is vitally important and relevant to applications such as mixing of air/fuel and chemical compounds; dispersion of plume and pollutant; V/STOL aerodynamics; wall cooling; etc. Studies of the past have made considerable progress towards the understanding of flow characteristics (e.g., Keffer and Baines, 1963; Pratte and Baines, 1967; Kamotani and Greber, 1972; Wright, 1977; Broadwell and Breidenthal, 1984; Sherif and Pletcher, 1989a) and flow structures (e.g., Moussa et al., 1977; Fric and Roshko, 1994; Kelso et al., 1996 and 1998; Haven and Kurosaka, 1996 and 1997; Smith and Mungal, 1998; Yuan et al., 1999; Lim et al., 2001). Of particular interest, four or more known vortical structures, i.e., horseshoe vortices, jet shear layer, wake structure, and counter-rotating vortex pair (CVP), are believed to play vital roles in the evolution of the jet. Extensive review on the past studies of jets in crossflow is summarized in Margason (1993).

Characteristics of a jet in crossflow that are indicative of mixing are its trajectory, penetration depth, decay, and spreading rate. Studies in the past have shown that the trajectory, physical dimension, and spreading rate of a jet in crossflow display the rd-scaling law; r is the effective jet-to-crossflow momentum flux ratio, defined as

$r = \left[(\rho_j U_j^2)/(\rho_{cf} U_{cf}^2)\right]^{1/2}$, where ρ is density, U is velocity, and the subscripts j and cf refer to jet and crossflow properties respectively, and d is diameter of the jet exit (Pratte and Baines, 1967; Broadwell and Breidenthal, 1984; and Smith and Mungal, 1998). Specifically, Pratte and Baines (1967) study a jet in crossflow with r ranged from 5 to 35 and find the correlation for the trajectory of the jet to be

$$\frac{y}{rd} = A\left(\frac{x}{rd}\right)^m,$$

where the Cartesian coordinates system employed is shown in Fig. (1), m = 0.28, and A = 2.63, 2.05, and 1.35 for the upper, center, and lower edge of the jet, respectively. Similarly, they also find the correlation for the spreading rate of the jet in the natural transverse direction η to be

$$\frac{\Delta\eta}{rd} = A\left(\frac{x}{rd}\right)^m,$$

where m = 0.4, and A = 0.92; and in the z direction to be

$$\frac{\Delta z}{rd} = A\left(\frac{x}{rd}\right)^m$$

where m = 0.4, and A = 1.25. Note that (ξ,η,ζ) is a natural coordinates system as illustrated in Fig. (1). Depending upon the quantity measured (e.g., velocity, temperature, scalar, etc.) and the method of measurement, different authors use slightly different definitions of the natural coordinates. Therefore, in this brief review, no attempt is made to reconcile the difference in the coordinates employed, and the natural coordinates system is loosely defined in Fig. (1). As a result, unless otherwise specifically stated, the reader is suggested to consult the cited references for more details.

Kamotani and Greber (1972) study unheated and heated jets in crossflow for jets with r ranged from 4 to 24 (r^2 from 15 to 570) and excess temperature from 0 °F to 400 °F over room temperature. They find that the jet motion is inertially dominated with buoyancy playing a minor role. Specifically, the velocity and temperature trajectories, defined as the loci of the corresponding maxima in the center plane, depend mainly upon r, with the temperature trajectory weakly depending upon the density ratio. In addition, they also find that the temperature trajectory falls below the velocity trajectory. They also show that the normalized temperature profiles, $(T - T_{cf})/(T_{max} - T_{cf})$, collapse onto a Gaussian error curve when plotted against the normalized transverse coordinate, $\eta/\eta_{0.5}$, where T is local temperature, T_{cf} is cross flow temperature, T_{max} is local maximum temperature, and $\eta_{0.5}$ is half width at half maximum. Similarly, Keffer and Baines (1963) study a jet in crossflow with r ranged from 2 to 10 and find the collapse of velocity profiles for $r \geq 4$ when the normalized velocity $(U - U_{cf})/(U_m - U_{cf})$ is plotted against $\zeta/\zeta_{0.5}$, where U is local velocity, U_{cf} is cross flow velocity, U_m is velocity at the jet center, ζ is the natural lateral coordinate, and $\zeta_{0.5}$ is the corresponding half width at half maximum.

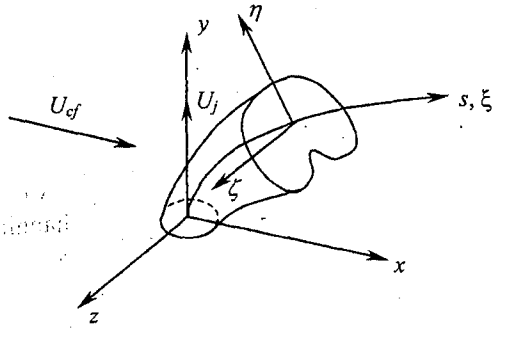

Fig. 1. Jet in crossflow and coordinates system.

Smith and Mungal (1998) study the concentration decay along the centerline coordinate s of a jet in crossflow with r ranged from 5 to 25. Note that s is defined as the locus of points in the center plane at which the maximum concentration value occurs on a line perpendicular to the local jet direction, see Fig. (1). It is found that, for jets with r ranged from 10 to 25, in the near field the centerline concentration of a jet in crossflow decays as

$s^{-1.3}$, faster than that of a free jet (s^{-1}); therefore, the near field corresponds to the region of enhanced mixing. On the other hand, in the far field it decays as $s^{-2/3}$, slower than that of a free jet; therefore, the far field corresponds to the region of reduced mixing, compared to a free jet. The transition from the region of enhanced mixing (near field) to the region of reduced mixing (far field) is found to be at the branch point $s/r^2d = 0.3$ or $x/r^2d \sim 0.2$. It is noted that the near field is the region of CVP formation and the far field is the region where the CVP is fully developed. This suggests that, although the CVP is the main mechanism for entrainment in the far field, the CVP itself does not enhance mixing as the centerline concentration decays only as $s^{-2/3}$ in comparison to s^{-1} of a free jet. Instead, the mechanism that enhances mixing should lie in the near field and may be related to the structural formation of the CVP. On the other hand, for the jet with r of 5, slightly different characteristics are observed. They suggest that the jet with $r = 5$ may belong to a different flow regime where wall effects and image vortices may be important.

Using Large-Eddy Simulation (LES), Yuan et al. (1999) study a jet in crossflow with r of 2.0 and 3.3. They show that the CVP is originated from a pair of quasi-steady 'hanging vortices' formed in the *skewed* or *oblique shear layer* which develops at each lateral edge of the jet. Their results also suggest that the spanwise rollers formed from the upstream and downstream edges of the jet shear layer and their interaction in the near field may provide dominant mechanism for entrainment and mixing.

To this end, attempts have been made to manipulate the characteristics of a jet in crossflow in order to enhance mixing by modification of the structures in the near field, predominantly via modification of the initial conditions. One method is the use of swirl, which can render both passive and active flow controls depending upon the method of delivering swirl. Kavsaoglu and Schetz (1989) study a swirling jet in crossflow with r of 2.2, 4, and 8, and *swirl ratios* (*Sr*) of 0.4 and 0.58. In this study, Kavsaoglu and Schetz define swirl ratio as the maximum peripheral velocity near the nozzle wall divided by the average axial velocity. This corresponds to *swirl numbers* (*S*) of 0.25 and 0.45 (after Niederhaus et al., 1997). Note that swirl number is defined as the ratio of the axial flux of angular momentum and the axial flux of axial momentum times the nozzle radius: $S = \left(\int rw\dot{m}\right)/\left(R\int u\dot{m}\right)$, where r is radial coordinate, u is axial velocity, w is azimuthal velocity, and R is nozzle radius. Kavsaoglu and Schetz find that swirl has stronger effect on wall-pressure distribution on a jet with lower momentum flux ratio and higher swirl. Specifically, swirl causes asymmetric wall pressure distribution, pressure generally being lower on the 'suction' side than on the 'pressure' side. Here, we borrow the nomenclature for the two lateral sides of the jet with respect to the center plane according to *aerodynamics of Magnus effect: suction side* refers to the lateral side at which the tangential velocity of the jet is in the same direction as the crossflow velocity; and pressure side, the opposite. At swirl ratio of 0.4, the effect of swirl on wall pressure is observed at r of 2 but diminished at r of 4. On the other hand, at swirl ratio of 0.58, the effect of swirl is still pronounced at r of 4 but diminished at r of 8. Detailed survey of mean velocity field at r of 4 shows that, the swirl ratio of 0.4 has little effect on the penetration depth, while that of 0.58 has pronounced effect. In addition, at the swirl ratio of 0.58, the asymmetric vortex pair is found; the vortex on the suction side has higher velocity and is closer to the wall. Yagci and Kavsaoglu (1993) use numerical simulation with turbulence models to simulate the swirling jet in crossflow of Kavsaoglu and Schetz (1989) at the swirl ratio of 0.58. Asymmetric nature of the flow field is predicted, but agreement in wall-pressure distribution is found only in limited region lying not too close and not too far from the jet.

Niederhaus et al. (1997) use Planar Laser-Induced Fluorescence (PLIF) to study a swirling jet in crossflow with r of 4.9, 7.6, and

11.1, and swirl numbers of 0, 0.08, 0.13, and 0.17. For limited range of swirl numbers investigated, they find the effect of swirl to be complex and dependent on velocity ratio. Generally, for low to moderate velocity ratios, they find the effect of swirl to increase with swirl number. Namely, at a fixed velocity ratio, when swirl is introduced and increased, symmetric kidney-shaped mean concentration field in the cross plane is found to be transformed into asymmetric comma-shaped field, with the lobe on the suction side decreasing in size and maximum concentration whereas the one on the pressure side increasing in size. The degree of asymmetry is found to increase with swirl with the maximum concentration located on the lobe on pressure side. In addition, the penetration depth is found to decrease with increasing swirl. At higher velocity ratio, however, these effects are significantly reduced. On the other hand, the decay of maximum mean concentration is not significantly affected by swirl.

From past studies, it can be seen that although the characteristics of a jet in crossflow has been rather well studied and considerable understanding has been gained, data on the effect of rotation, or swirl, on the characteristics of the jet are still far less. It is also evident from past studies (Smith and Mungal, 1998; Yaun et al., 1999) that an attempt to modify the evolution and characteristics of a jet in crossflow should be made via modification of the near-field flow structures. In this respect, one issue in case of the effect of swirl and swirl as a means for manipulating flow structure is related to the mechanism by which pertinent flow structures are generated and the effect of the generation mechanism on the evolution and characteristics of the jet. Of particular interest in this case is a pair of counter-rotating vortices, or CVP, which is suggested by Yuan et al. (1999) to originate from a skewed shear layer on each lateral side of the jet. It seems likely then that manipulation of this mechanism may lead to structural change in the flow; this is already evident from the works of Kavsaoglu and Schetz (1989) and Niederhaus et al. (1997). Nonetheless, in these two studies, swirl is generated by paddle or tangential injection, the mechanisms in which the tangential velocity of the jet at the nozzle lip is zero and which produce no net circulation around the jet. In this regard, from flow manipulation viewpoint, these methods cannot render direct and local control over the tangential velocities at the lateral edges of the jet and, as a result, over the generation and strength of the skewed shear layers for it is obscured by the thickness δ of and the vorticity in the boundary layer, see Fig. (2).

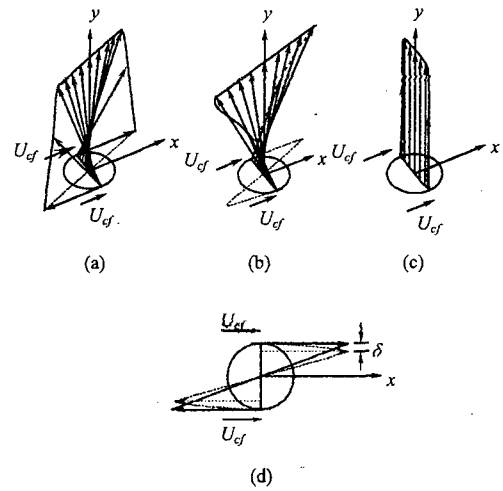

Fig. 2. Schematics illustrate initial velocity profiles of jets in crossflow: swirling jets generated by (a) non-zero tangential velocity/non-zero circulation method (rotating-pipe) and (b) by zero tangential velocity/zero circulation method; (c) non-swirling jet; (d) comparison of the tangential velocity profiles for (a) and (b).

In this study the effect of swirl on characteristics of a jet in crossflow is therefore investigated with a direct means of controlling the tangential velocity at the edge of the jet. Specifically, a rotating pipe is used for swirl generation. Hence, the method renders a direct control over the tangential velocity of the jet at

the interface to the crossflow and, as a result, over the generation and strength of the skewed shear layers at the lateral edges of the jet. In addition, this method renders control over the net circulation around the jet. The difference between the initial profiles of jets generated by the two methods: one with tangential velocity and net circulation and one without, is illustrated schematically in Fig. (2).

In order to investigate the characteristics of a jet in crossflow under the influence of swirl with non-zero circulation, heated swirling jet generated from a rotating pipe is used and the temperature distribution in the near field downstream of the jet is surveyed. Experiment is conducted at a fixed effective jet-to-crossflow momentum ratio. This paper reports our preliminary results on the trajectory and decay of maximum centerplane-temperature and some detailed results on the temperature distributions in the crossplane.

2. Experimental Setup

The experiment is conducted in the Fluid Mechanics Research Laboratory (FMRL), Department of Mechanical Engineering, Faculty of Engineering, Chulalongkorn University. The main facilities include the new 100x100 cm^2 blower tunnel and a 32-mm diameter heated swirling-jet setup. The details of the experiment are as follows.

2.1. Flow facility

The wind tunnel, shown schematically in Fig. (3), is used for generating a crossflow. The main components of the tunnel from upstream to downstream are centrifugal blower, flexible duct, first-stage adaptor diffuser, main diffuser, settling chamber, contraction, and test section. The centrifugal blower is an airfoil-blade backwardly-curved centrifugal blower which is driven by a 30 kw motor and a variable frequency inverter. The blower has an exit cross section of (W x H) 80x90 cm^2. The flexible duct is used for isolating the remaining sections of the tunnel from vibration of the blower; the first-stage adaptor diffuser for adapting the exit cross section of the blower to match that of the inlet of the main diffuser. The main diffuser is a symmetric straight-walled diffuser with 160x160 cm^2 inlet, 300x300 cm^2 exit, and 160 cm length (an area ratio of 3.5 and a total diverging angle of 47°). Flow conditioning devices in the diffuser include four steel perforated plates with hole (mm) x pitch (mm) of 25x32 and one of 2x3, located at 0, 25, 50, 80, and 110 cm from the inlet, respectively. The settling chamber is of 300x300 cm^2 in cross section and 217 cm in length. Flow conditioning devices in the settling chamber include, from upstream to downstream, a pair of stainless steel wire-gauze screens of 50x36 (mesh x SWG) and five aluminum wire-gauze screens of (16x18)x31, uniformly spaced at 31 cm. The first of the pair of wire-gauze screens is located right at the settling chamber inlet, hence at the diffuser exit. For budgetary reason, the tunnel was designed without a honeycomb. Instead, the pair of fine screens are employed in order to remove swirl. The contraction has an exit cross section of 100x100 cm^2 nominal (98.5x98.5 cm^2 actual), hence the contraction area ratio of nine. The profile of the contraction is fourth-degree polynomial with the inflection point located at 2/3 of the profiled length, which is 300 cm long, from the inlet. Although the profiled length of the contraction is 300 cm long, a straight extension of 10 cm long is added at each end, making the total length of 320 cm.

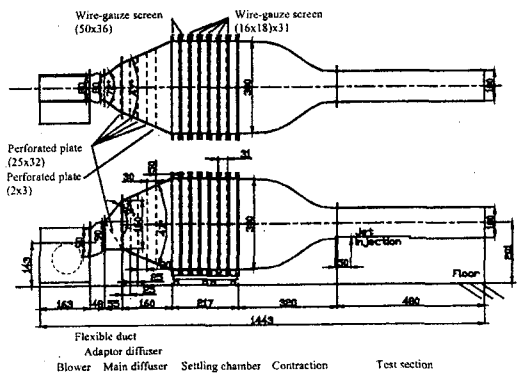

Fig. 3. Schematic of the wind tunnel. (Dimensions are in cm.)

The test section consists of two sections, each is 98.5x98.5 cm^2 in cross section and 240 cm long. The two side walls and the upper wall of the first section are made from acrylic plates. The bottom wall, under which the jet is flushed mounted, is made from steel plate of 97.5 cm wide, 240 cm long, and 5 mm thick. The plate is mounted at the center of the span, raised by 4.5 cm above the test section floor level, and inserted by 10 cm into the contraction measured from the contraction exit plane. As a result, a gap of 0.5 cm in width is created along each side edge of the plate to reduce the effect of corner flow, and another of 4 cm in height at the leading edge of the plate to remove the boundary layer on the lower contraction wall. Thus, the flow cross section of the first section is 98.5 cm in width and 94 cm in height. The second section has a flow cross section of 98.5x98.5 cm^2 and its four walls are made from acrylic plates.

The installation of the heated swirling-jet setup is shown schematically in Fig. (4). The main components of the setup from upstream to downstream are centrifugal blower, flexible duct, flow monitoring section, heating chamber, and rotating-pipe jet section. The centrifugal blower is a backwardly-curved blade centrifugal blower driven by a 1.5 kw motor. The flexible duct is used for isolating the remaining sections of the setup from vibration of the blower. The flow monitoring section includes a butterfly valve for adjusting and an orifice for monitoring the flow rate. The piping from the blower to the heating chamber is appropriately sized. The heating chamber is 30x30 cm^2 in cross section and 120 cm in length with an inlet of 12.5 cm in diameter. At the inlet flange, a 50x36 stainless steel wire gauze screen is employed to filter dust form the air stream. The chamber is divided into 6 sub chambers of equal width, each is separated by steel perforated plates with hole (mm) x pitch (mm) of 10x15. Three w-type finned electric heaters, each of 2 kw, are installed at the center of the first three upstream sub chambers. In order to be able to adjust the heating rate, the three heaters are connected to the main electrical supply (3-phase/380V/50 Hz.) through a three-phase/four-wire, 0-480V/30A, voltage transformer.

The rotating-pipe jet section is basically a pipe assembly supported by bearings along its length and driven to rotate about its axis by motor and pulley. It is divided into three sections, each is made from stainless steel tube with inner diameter (d) of 32 mm and outer diameter of 42 mm: the first (upstream) section is 300 mm (9.4d) long, the second 510 mm (15.9d), and the third 450 mm (14d), connected together by collars. The first section is an empty tube. The second is packed with brass tubes of 4 mm in inner diameter, 4.5 mm in outer diameter, and length of the section in length, i.e., 15.9d. At each end of the section is installed 30x35 stainless steel wire-gauze screen. Thus, the second section, packed inside with brass tubes, functions as a rotating honeycomb and exerts rotational motion to the air stream inside as it rotates. The third section provides flow conditioning as it is installed with three 30x35 stainless steel wire-gauze screens at a distance of 60 (1.9d) mm apart from the honeycomb exit, thus leaving a clear length from the last screen to the jet exit of 270 mm (8.4d). Rotational motion of the rotating-pipe jet section is provided by a 2-hp motor and a frequency inverter through belt and pulley. Seal at the connection between the rotating pipe and the tunnel floor is provided by a graphite bush and a mechanical seal.

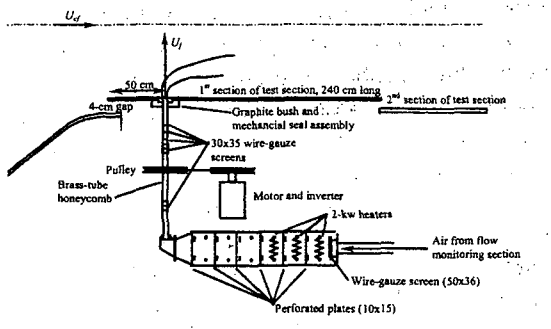

Fig. 4. Schematic of the heated swirling-jet setup and its installation.

2.2. Flow condition

A set of experiments is performed at the crossflow velocity of 1.8 m/s, area-averaged jet velocity of 8.0 m/s (centerline velocity of 9.6 m/s), crossflow temperature of 30 °C, and area-averaged jet temperature of 70 °C (centerline temperature of 75 °C). This results in the jet Reynolds number of 1.2×10^4; the effective momentum flux ratio r of 4.1; the densimetric Froude number Fr, defined as $Fr = \left[(\rho_{cf} - \rho_j)gd\right)/\left(\rho_{cf}U_{cf}^2\right)\Big]^{1/2}$ and is a measure of relative magnitude of buoyancy force and inertia, of 0.1; and Fr/r, which results in $\left[(\rho_{cf} - \rho_j)gd\right)/\left(\rho_j U_j^2\right)\Big]^{1/2}$, of 0.025.

In order to investigate the effect of swirl, the experiments are performed at four swirl ratios ranged from no swirl to high swirl: Sr = 0 (no swirl), 0.17, 0.52, and 0.82. For ease of reference, these cases shall be referred to as Sr0, Sr17, Sr52, and Sr82 respectively. Note that the swirl ratio is defined here as the ratio of peripheral pipe speed to the average axial velocity.

2.3. Measurement

For each case, a set of measurements is made for initial condition and maximum centerplane-temperature trajectory and decay.

Initial velocity and temperature profiles of the jet in each case are measured on the exit plane of the jet while the crossflow is turned off. Pitot probe is used for the measurement of initial velocity profile for case without swirl (Sr0); three-tube cobra probe, for cases with swirl. Pitot probe in these measurements is laboratory-built from a hypodermic needle with inner diameter of 0.8 mm and outer diameter of 1.2 mm. Three-tube cobra probe is also laboratory-built from hypodermic needles with inner diameter of 0.4 mm and outer diameter of 0.6 mm. The probe has a total apex angle of 60°. The construction of the probe can be found in Chue (1975). The probes are calibrated in house at room temperature and correction in the results is made for density effect from temperature data. Copper-constantan thermocouple (type T) is used for the measurement of initial temperature profile.

For the case without swirl (Sr0), the measurements are made along the x' and z'-axes, where prime denotes the coordinate axes similar to those in Fig. (1) but fixed to the jet pipe. Because the probe access is from the side wall (+z wall), however, the measurements along the x'-axis are made by rotating the pipe by 90° from the test configuration. For the cases with swirl, the measurements are made along the z-axis.

For all cases, the maximum centerplane-temperatures together with their locations are measured at x/rd = 0.25, 0.5, 0.75, 1, 1.5, and 2. The measurements are made with copper-constantan thermocouple (type T). The uncertainty in measurement of temperature is estimated to be $\pm$ 0.5 °C.

3. Results

3.1. Initial conditions

Initial condition of both the crossflow and the jet flow were investigated and the results are as follows.

Crossflow condition

The uniformity of the crossflow was determined by the measurement of mean velocity distribution in the cross plane located at x = -15 cm and outside the boundary layers. The measurement was made with a pitot probe, at the freestream velocity of approximately 8 m/s, and with the spatial resolution of 10 cm x 10 cm points. The result shows that the non-uniformity of the tunnel at the measured speed and resolution lies within 7.89 $\pm$ 0.05 m/s, or $\pm$ 0.6%. Taking the uncertainty and the spatial resolution of measurement into account, it is estimated that the non-uniformity of the tunnel lies well within $\pm$ 1%.

The measurement of the incoming boundary layer at mid span of the floor and x = -10 cm (-3.1d or -0.8rd) indicates the boundary layer is fairly laminar with $\delta_{0.95}$, the 95% boundary layer thickness, of approximately 3 mm.

At this point, some discussion is in order. At present, the uniformity and the boundary layer of the crossflow at the test velocity, i.e., 1.9 m/s, could not be determined directly owing to the availability, or lack thereof, of the measuring instrument that can measure low velocity range accurately. Therefore, throughout the experiment, the speed of the tunnel blower was fixed and the crossflow velocity was measured and monitored with a pitot probe. No significant variation in the crossflow velocity was detected.

Jet condition

The initial velocity profiles for all cases are shown in Figs. 5(a) and (b). Note that these data are corrected for the variation in density but not for the probe size. In these figures, the normalized axial velocity distributions along the x'- and z'-axis for case Sr0 and the normalized axial and tangential velocity distributions for cases with swirl are shown; the axial components are normalized by the corresponding maximum values, $u_{\max}$, while the tangential components are normalized by the corresponding peripheral speeds of the pipe, w_p. The result shows that the axial velocity profiles for all cases are similar: top hat with slight asymmetry. In addition, slight dip in the profile at the center is observed for cases with swirl. The normalized tangential profiles for cases with swirl are fairly linearly distributed along the radial direction, indicating the characteristics of a rigid-body-like rotation; nonetheless, slight deviation can be observed. The best linear fit, also shown in the figure, indicates that the mean rotational speed is lower than the rigid-body rotational speed of the pipe by less than 2% for cases Sr52 and Sr82 and by less than 5% for case Sr17.

The corresponding initial temperature profiles are shown in Fig. (5c) as normalized temperature coefficient $(T - T_a)/(T_{\max} - T_a)$, where T is local jet temperature, T_{max} is the corresponding maximum value, and T_a is surrounding temperature. Note that the initial conditions are determined in the absence of crossflow. As is clearly seen, naturally the initial temperature profiles are more developed than the corresponding velocity profiles.

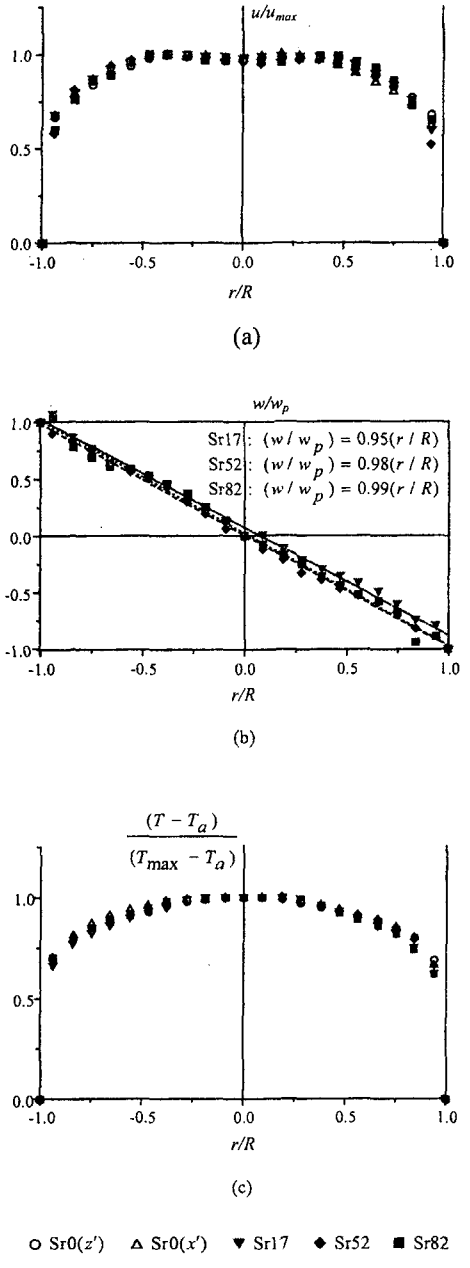

Fig. 5. Initial velocity and temperature profiles at the jet exit; (a) axial velocity, (b) tangential velocity, (c) temperature.

3.2. Maximum centerplane-temperature trajectory and decay

Figure (6) shows the maximum centerplane-temperature trajectory for case without swirl, i.e., case Sr0. The result is shown in *rd*-scale with the curve fit given by the power law: $(y_T / rd) = A(x / rd)^m$, where y_T indicates the traverse position of point of maximum centerplane-temperature, and constant A and m are found to be 1.3 and 0.3, respectively. The figure also shows the corresponding correlations (at the same density ratio) for maximum centerplane-temperature (y_T) and -velocity (y_U) of Kamotani and Greber (1972) for comparison. As the figure shows, the present data lie slightly above the temperature trajectory and below the velocity trajectory as given by the two correlations.

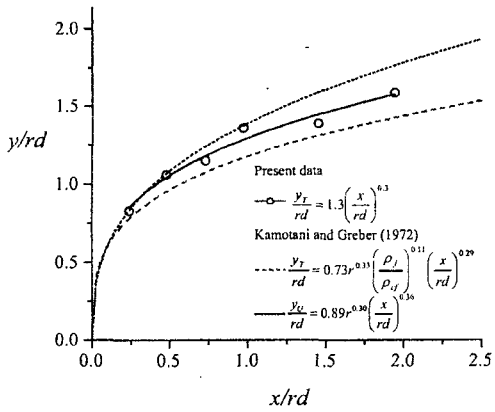

Fig. 6. Maximum centerplane-temperature trajectory for case Sr0.

When swirl is imposed, scatter in data and trajectories are observed as shown in Fig. (7). As seen in the figure, no obvious trend can be discerned, and the scatter in data can be accounted for by experimental uncertainty. Nonetheless, this is not to be interpreted as that a jet in crossflow is not affected by swirl; it simply means that the maximum centerplane-temperature trajectory is not significantly affected by swirl within the present ranges of experimental parameters. We shall investigate further on this by detailed measurement of temperature distribution in the cross plane below.

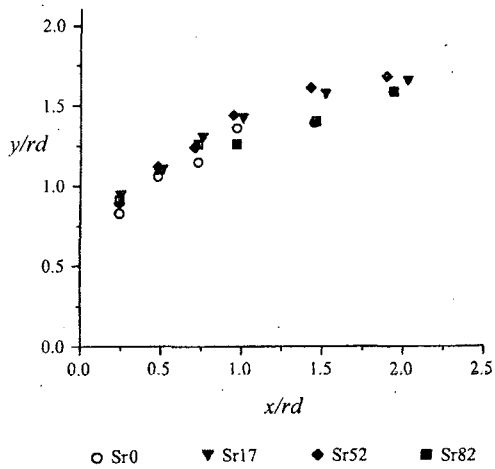

Fig. 7. Maximum centerplane-temperature trajectories for all cases.

For maximum centerplane-temperature decay, we plotted the *global coefficient of temperature*, C_{TG}, defined as

$$C_{TG} = \frac{T - T_{cf}}{T_J - T_{cf}},$$

where T is local temperature, T_J is area-averaged temperature of the jet at the jet exit, and T_{cf} is crossflow temperature, for the maximum center-plane temperature ($T = T_{max}$ in centerplane). The uncertainty in C_{TG} is conservatively estimated to be $\pm$ 0.05. The results are shown in Fig. (8). Although slight deviation from case Sr0 is observed in Fig. (8a), in which the curve fit for Sr0 is also shown, the deviation is comparable to experimental uncertainty and, at this point, is deemed to be insignificant. Data fits shown in Fig. (8b) as a power law, $C_{TG} = A(x / rd)^{-m}$, indicate that the decay rate lies approximately in the range of –0.49 to –0.55. It is interesting to note that the maximum excess centerplane-temperature decays to approximately 40% and

15% of the original value at the jet exit within the first 0.25*rd* and 2*rd*, respectively.

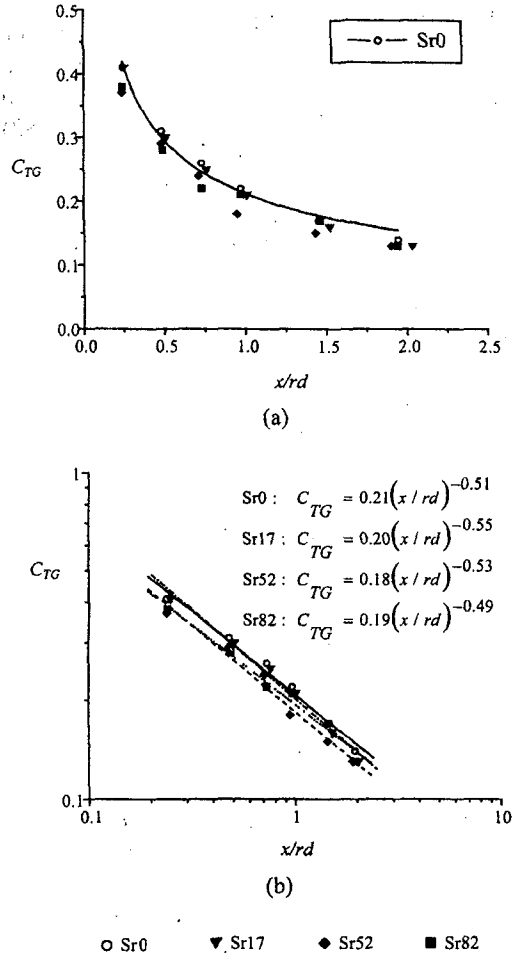

Fig. 8. Decay of maximum centerplane-temperature.

3.3. Temperature distribution in a cross plane

In order to further clarify the effect of swirl, we make detailed measurement of the temperature distribution in the crossplane (*y-z* plane) at $x/rd = 0.5$. The results are shown in Fig. (9) in terms of the contour of global temperature coefficient (C_{TG}) on the *rd*-normalized crossplane, with the uncertainty estimate of $\pm$ 0.05 as before.

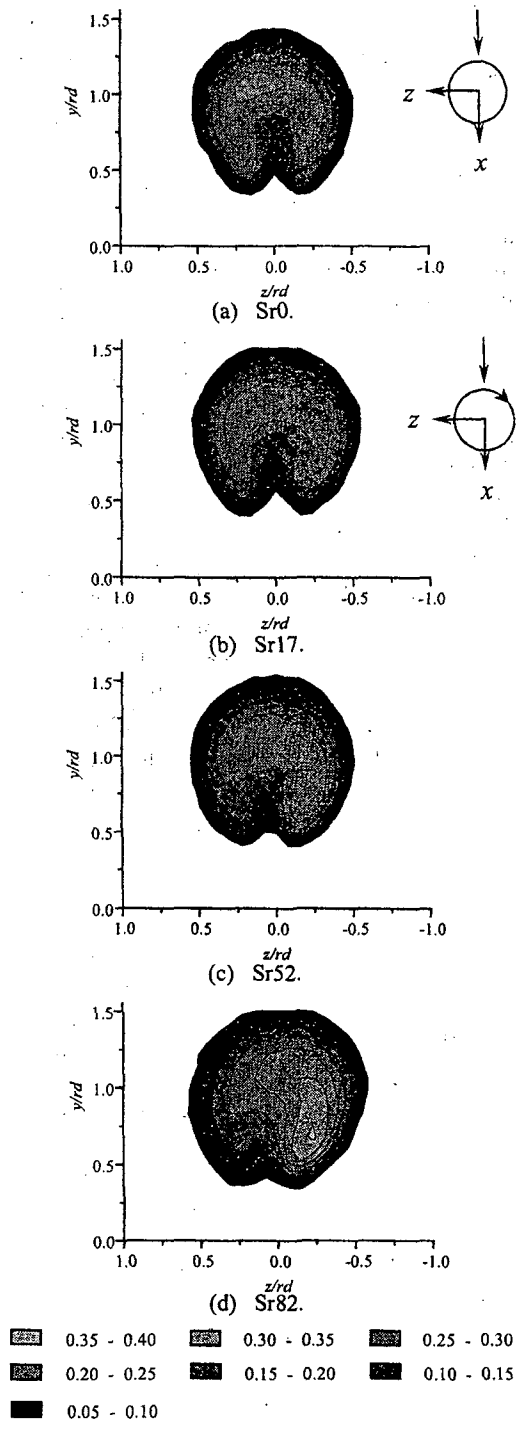

Fig. 9. Temperature distributions in the *rd*-normalized crossplane at $x/rd = 0.5$ (C_{TG}, looking upstream).

The view in Fig. (9) is as if the reader was looking upstream towards the jet, i.e., *end view*. The aspect ratio of the scale of the figures is approximately one, thus the figures show qualitatively the relative shape and size as well as the position of the jet with respect to ground ($y = 0$). Small diagrams are also drawn at the upper right corner to indicate the relative direction of rotation of the jet (if applicable) as viewed from *top*. For example, for swirling cases, the suction side of the jet lies to the right; and the pressure side, to the left. Note also that, according to the criterion of Smith and Mungal (1998), the branch point that separates the near field from the far field in this case is at $x/rd = 0.8$; hence the distributions shown here are in the near field.

In case Sr0, the kidney-shape structure is observed. In addition, slight asymmetry of the region of high and maximum temperature is observed to lean towards the left. As mentioned by Smith and Mungal (1998), creating a symmetric jet in crossflow is not regularly accomplished in laboratory study. On the other hand, it is interesting to note that, albeit an obvious asymmetry in the region of high temperature, the envelop of low temperature is relatively and fairly symmetric.

When swirl of significant strength (Sr52 and Sr82) is imposed on the jet in the direction shown, the asymmetry of the region of high and maximum temperature moves opposite under the influence of swirl, i.e., towards the right. In other words, the region of high and maximum temperature is located on the suction side. Nonetheless, it is noted that, as before, a fairly symmetric in shape of the low temperature envelop similar to the case without swirl is persistent and, thus, observed.

As a result, the symmetric low temperature envelop together with the influence of swirl on the high temperature region create a relatively high temperature gradient region on the suction side and a corresponding relatively low temperature gradient region on the pressure side, both when comparisons are made between the two sides of the same case and between cases. In addition, as swirl increases, the degrees of asymmetry in temperature distribution increase.

Furthermore, in terms of maximum temperature, it is noted that the maximum temperature decreases with swirl at low to moderate swirl (Sr0 to Sr52) but increases with swirl at moderate to high swirl (Sr52 to Sr82). This is, however, slight in comparison to the experimental uncertainty. Nonetheless, for the case of high swirl (Sr82), temperature survey at $x/rd = 0.25$ shows that this is the case.

4. Discussion

Of particular interest in these results are the corresponding regions of high and low temperature gradient on the suction and pressure sides, respectively. This is thought to be the consequence of the mechanism by which a skewed shear layer is generated on each lateral edge of the jet and, as a result, the velocity difference across the shear layer, or the *strength* of the shear layer, see Yuan et al. (1999). Specifically, on the suction side, the tangential velocity of the jet is in the same direction as the crossflow velocity (see Fig. 2). This causes reductions in skew angle and velocity difference across the shear layer and results in slower development of the shear layer and higher temperature gradient. On the contrary, on the pressure side, the tangential velocity of the jet is in the opposite direction to the crossflow velocity, thus causing increases in skew angle and velocity difference and resulting in faster development and lower temperature gradient. The effect of increase in swirl ratio on the configuration of the skewed shear layer on each lateral edge of the jet is shown schematically in Fig. 10. Note that the effect of boundary layer thickness in the streamwise direction is neglected in this figure. Also, it is interesting to note that, in contrast, Niederhaus et al. (1997), using zero tangential velocity/zero circulation method for swirl generation and measuring concentration, observed the region of high and maximum concentration on the *pressure* side.

Another interesting point as pointed out in the last section is the fact that, albeit the asymmetry in the high temperature region, the

low temperature envelop is relatively and fairly symmetric, with or without swirl. In addition, the global parameters such as maximum centerplane-temperature trajectory and decay, and the shape and size of low temperature envelop are little influenced by swirl. This suggests that, even though the detailed development of a jet in crossflow is obviously and strongly affected by swirl, the overall configuration is predominantly governed by the effective jet-to-crossflow momentum ratio, with little influence from swirl. At this point, it is noted that the injection of a jet into a stream of crossflow adds axial flux of axial momentum into the flow while the injection of a swirling jet generated by rotating pipe also adds axial flux of angular momentum.

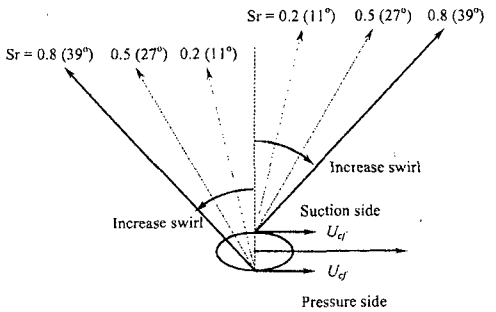

Fig. 10. Effect of increase in swirl ratio at fixed effective jet-to-crossflow momentum ratio on skew angle on suction and pressure sides.

5. Conclusions

This paper is a preliminary report of our study on non-zero-circulation swirling jet in crossflow. In this program of study, a heated swirling jet generated from a rotating pipe is used and the temperature distribution in the near field downstream of the jet is surveyed. The experiment is conducted at a fixed effective jet-to-crossflow momentum ratio. In this paper, the global parameters, namely the maximum centerplane-temperature trajectory and decay, as well as some detailed temperature distribution in a crossplane are reported.

The results indicate that, within the present range of parameters, swirl has little influence on the two global parameters when compared to the effect of the effective jet-to-crossflow momentum ratio. This can be seen from the fact that the maximum centerplane-temperature trajectories (and decay) for the wide range of swirl ratios investigated (0 to 0.82) collapse fairly well onto a single *rd*-correlation law found earlier for a non-swirling jet (Pratte and Baines, 1967; Kamotani and Greber, 1972).

On the other hand, detailed measurements of temperature distribution in the crossplane reveal the pronounced effect of swirl on the jet structure. Namely, swirl causes asymmetry in the jet structure and in the temperature distribution within the jet. Specifically, swirl causes a region of high and maximum temperature and temperature gradient to develop on the *suction* side, and a corresponding region of low temperature and temperature gradient on the *pressure* side. This is attributed to the development, and the contrasting effect of swirl velocity on the development, of a skew mixing layer on each lateral edge of the jet.

In regard to the asymmetry of the distribution of temperature within the jet, two interesting points are pointed put. Firstly, even though swirl causes asymmetry in temperature distribution within the jet as just mentioned, the low temperature envelop of the jet is relatively symmetric and the global parameters are little influenced by swirl. These seem to suggest, to certain extent, the distinctive roles and effects of the effective jet-to-crossflow momentum ratio (r) and of swirl (Sr). Secondly, in contrast to present results, Niederhaus et al. (1997), using zero tangential velocity/zero circulation method for swirl generation and measuring concentration, observed the region of high and maximum concentration on the *pressure* side.

Acknowledgements

Research funds from The National Energy Policy Office (NEPO) and The Ministry of

University Affairs under the Grants for Graduate Research 2000 for the first author, and from The ASAHI Glass Foundation under the Overseas Research Grant 2000 for the second author are gratefully acknowledged. Assistance from Sidtipong Sathapornnanon is greatly appreciated and acknowledged.

References

1. Broadwell, J. E., and Breidenthal, R. E., 1984, "Structure and mixing of a transverse jet in incompressible flow," *J. Fluid Mech.*, Vol. 148, pp. 405-412.
2. Chue, S. H., 1975, "Pressure probes for fluid measurement," *Prog. Aerospace Sci.*, Vol. 16, No. 2, pp. 147-223.
3. Fric, T. F., and Roshko, A., 1994, "Vortical structure in the wake of a transverse jet," *J. Fluid Mech.*, Vol. 279, pp. 1-47.
4. Haven, B. A., and Kurosaka, M., 1996 "The effect of hole geometry on lift-off behavior of coolant jets," AIAA Paper No. 96-0618.
5. Haven, B. A., and Kurosaka, M., 1997, "Kidney and anti-kidney vortices in crossflow jets," *J. Fluid Mech.*, Vol. 352, pp. 27-64.
6. Kamotani, Y., and Greber, I., 1972, "Experiments on a turbulent jet in a cross flow," *AIAA J.*, Vol. 10, No. 11, pp. 1425-1429.
7. Kavsaoglu, M. S., and Schetz, J. A., 1989, "Effects of swirl and high turbulence on a jet in a crossflow," *J. Aircraft*, Vol. 26, No. 6, pp. 539-546.
8. Keffer, J. F., and Baines, W. D., 1963, "The round turbulent jet in a cross-wind," *J. Fluid Mech.*, Vol. 15, pp. 481-496.
9. Kelso, R. M., Lim, T. T., and Perry, A. E., 1996, "An experimental study of round jets in cross-flow," *J. Fluid Mech.*, Vol. 306, pp. 111-144.
10. Kelso, R. M., Lim, T. T., and Perry, A. E., 1998, "New experimental observations of vortical motions in transverse jets," *Phys. Fluids*, Vol. 10, No. 9, pp. 2427-2429.
11. Lim, T. T., New, T. H., and Lou, S. C., 2001, "On the development of large-scale structures of a jet normal to a crossflow," *Phys. Fluids*, Vol. 13, No. 3, pp. 770-775.
12. Margason, R. J., 1993, "Fifty years of jet in cross flow research," in *Computational and Experimental Assessment of Jets in Cross Flow*, AGARD-CP-534.
13. Moussa, Z. M., Trischka, J. W., and Eskinazi, S., 1977, "The near field in the mixing of a round jet with a cross-stream," *J. Fluid Mech.*, Vol. 80, pp. 49-80.
14. Niederhaus, C. E., Champagne, F. H., and Jacobs, J. W., 1997, "Scalar transport in a swirling transverse jet," *AIAA J.*, Vol. 35, No. 11, pp. 1697-1704.
15. Pratte, B. D., and Baines, W. D., 1967, "Profiles of the round turbulent jet in a cross flow," *J. Hydraulics Div., ASCE*, November, 1967, pp. 53-64.
16. Sherif, S. A., and Pletcher, R. H., 1989a, "Measurements of the flow and turbulence characteristics of round jets in crossflow," *J. Fluids Eng.*, Vol. 111, 165-171.
17. Smith, S. H., and Mungal, M. G., 1998, "Mixing, structure and scaling of the jet in crossflow," *J. Fluid Mech.*, Vol. 357, pp. 83-122.
18. Wright, S. J., 1977, "Mean behavior of buoyant jets in a crossflow," *J. Hydraulics Div., ASCE*, May, 1977, pp. 499-513.
19. Yagci, H., and Kavsaoglu, M. S., 1993, "Navier-Stokes analysis of a swirling jet in crossflow," in *Computational and Experimental Assessment of Jets in Cross Flow*, AGARD-CP-534.
20. Yuan, L. L., Street, R. L., and Ferziger, J. H., 1999, "Large-eddy simulations of a round jet in crossflow," *J. Fluid Mech.*, Vol. 379, pp. 71-104.